

Pre-clinical Evaluation of Implicit Deformable Models for Three-dimensional Segmentation of Brain Aneurysms in CTA

Monica Hernandez^a, Rosario Barrena^b, Gabriel Hernandez^b,
Guillermo Sapiro^c and Alejandro F. Frangi^{*a}

^aVisual Information Technologies (VIT) Lab, Aragon Institute of Engineering Research,
University of Zaragoza, Ada Byron Bldg. D2.03, Maria de Luna 1, E-50018 Zaragoza, Spain

^bAragon Institute of Health Sciences, Zaragoza, Spain

^cUniversity of Minnesota, Minneapolis, USA

ABSTRACT

Knowledge of brain aneurysm dimensions is essential during the planning stage of minimally invasive surgical interventions using Guglielmi Detachable Coils (GDC). These parameters are obtained in clinical routine using 2D Maximum Intensity Projection images from Computed Tomographic Angiography (CTA). Automated quantification of the three dimensional structure of aneurysms directly from the 3D data set may be used to provide accurate and objective measurements of the clinically relevant parameters. The properties of Implicit Deformable Models make them suitable to accurately extract the three dimensional structure of the aneurysm and its connected vessels. We have devised a two-stage segmentation algorithm for this purpose. In the first stage, a rough segmentation is obtained by means of the Fast Marching Method combining a speed function based on a vessel enhancement filtering and a freezing algorithm. In the second stage, this rough segmentation provides the initialization for Geodesic Active Contours driven by region-based information. The latter problem is solved using the Level Set algorithm. This work presents a comparative study between a clinical and a computerized protocol to derive three geometrical descriptors of aneurysm morphology that are standard in assessing the viability of surgical treatment with GDCs. The study was performed on a data base of 40 brain aneurysms. The manual measurements were made by two neuroradiologists in two independent sessions. Both inter- and intra-observer variability and comparison with the automated method are presented. According to these results, Implicit Deformable Models are a suitable technique for this application.

Keywords: brain aneurysm, CTA, segmentation, Implicit Deformable Models, Geodesic Active Contours, Level Set, Fast Marching, Vessel Enhancement Filter.

1. INTRODUCTION

Brain aneurysm is a potentially serious cerebral pathology due to eventual risk of intra-cerebral bleeding. Studies asserts that it has an incidence between 0.2 and 8.9% being more frequently in women in the 5th-7th decade of life.^{9, 12, 22, 25} The most serious complication happens when the aneurysm breaks, since this has fatal consequences in 2.6 – 9.8% of the patients and serious consequences in 10.9% of the patients due to intra cranial bruise, subsequent recurrent bleeding, hydrocephaly and spasms in brain vessels.^{5, 15, 17}

In the last years, there has been a growing trend to practise minimally invasive endovascular procedures. In patients with aneurysm rupture, these techniques stabilize the patient and facilitate further more aggressive treatments with the purpose of preventing the spasm after the intra-cerebral bleeding. Aneurysm coiling with Guglielmi Detachable Coil (GDC) is probably the most widespread method for permanent embolization. It consists on the placement of coils inside the aneurysm using coaxial catheters and micro catheters introduced through the femoral artery. They promote blood coagulation inside the aneurysm avoiding blood flow and pressure thus hampering its rupture.⁸

A correct placement of the GDC inside the aneurysm is crucial for the success of the treatment, for which it is desirable to have pre-surgical knowledge of the aneurysm dimensions as well as the three-dimensional

* Corresponding author: afrangi@unizar.es

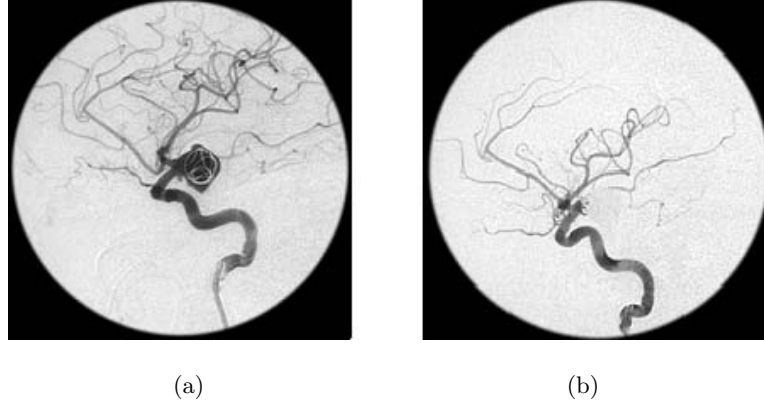


Figure 1. Digital Subtraction Angiography image of an embolized aneurysm using GDC coils. (a) Introduction of a GDC coil inside the aneurysm by catheterization. (b) Final result of the embolization.

morphology of the surrounding arteries. Particularly, it has been shown that the knowledge about the maximum neck diameter and the main axis dimensions of the aneurysm play an important role in the selection of patients and materials for an appropriate treatment.³

Digital Subtraction Angiography (DSA) is considered the gold standard criterion for the detection and representation of brain aneurysms. However, other fast and less invasive acquisition techniques like Computed Tomography Angiography (CTA) or Magnetic Resonance Angiography (MRA) are also used as a complementary method for this aim.^{1,24} For the obtaining of the aneurysm dimensions a reconstruction of the region of interest is extracted from the CTA or MRA data. It is usual in clinical practise to use Maximum Intensity Projection (MIP) images. This reconstruction method provides a two-dimensional image of the three-dimensional data in an angle optimal according to a specialist. Manual measurements are then carried out on the basis of this 2D image. The selection of the optimal angle introduces a high degree of subjectivity to the quantification of the aneurysm. It is often difficult to determine the depth relationships between the aneurysm and the surrounding and sometimes overlapping vessels, thus yielding wrong measurements owing to difficulties in image interpretation. For a correct interpretation of the three dimensional aneurysm morphology and the automatized extraction of accurate dimensions, it would be highly desirable to count with computerized segmentation techniques.

Most approaches used for the segmentation of vascular structures in CTA and MRA images belong to the class of Deformable Models. Frangi et al.⁶ compute the central axis of the artery which is modelled by a cylinder with this axis. Van Bemmelen et al.²³ also compute the central axis of the artery and use it as initialization for the Level Set Algorithm. Level Set Theory has also been used by Subasic et al.²⁰ in the segmentation of Aortic Abdominal Aneurysms. In the last years, Implicit Deformable Models have been successfully used in the extraction of the cerebral vascular tree^{13,14} and segmentation of brain⁴ aneurysms. Nevertheless, there is a lack of large and proper evaluation studies reporting on the accuracy of these computerized techniques for segmenting brain aneurysms in clinical data sets.

The goal of this paper is to present a pre-clinical validation of a segmentation method in a database of 40 brain aneurysms placed in the Circle of Willis. For this aim, we have used the segmentation technique based on Implicit Deformable Models due to its flexibility for segmenting complex structures. This paper presents a comparative study between a clinical and a computerized protocol to derive three geometrical descriptors of aneurysm morphology that are standard in assessing the viability of surgical treatment with GDCs. The manual measurements were made by two neuroradiologists in two independent sessions. Both inter- and intra-observer variability and comparison with the automated method are presented. The clinical parameters of study are the neck diameter and the main axis of the aneurysms.

The paper is organized as follows. Section 2 explains the devised segmentation method. Section 3 describes the materials and methods for validation. The results of the validation study are reported in Section 4. The discussion of the results is presented in Section 5. Finally, Section 6 provides some concluding remarks.

2. IMPLICIT DEFORMABLE MODELS FOR ANEURYSM SEGMENTATION

Using the ideas of Level Set theory, a two-stage segmentation algorithm is devised. In the first stage, a fast and rough segmentation is obtained by means of the Fast Marching Method. The speed used is based on a vessel enhancement filter. The output of the Fast Marching Algorithm is an image called *action map* with an abrupt jump of the time values in a neighborhood of the edges of the aneurysm and surrounding vessels. This allows us to extract a pre-segmentation of the aneurysm using a threshold of the action map. In images where there are other structures, the Fast Marching Algorithm is combined with a freezing algorithm.

In the second stage, the pre-segmentation is used as initialization for Geodesic Active Contours model. We use a modified partial differential equation for the model as follows. The pre-segmentation defines two regions on the image domain. The grey values belonging to these regions are modelled by Gaussian distributions. A constant speed based on these descriptors is added to the motion of the model equation. The Level Set Algorithm is used to track the motion of the embedding function. The final segmentation is the zero level set of the embedding function.

2.1. FAST MARCHING METHOD

Let Γ_0 be a curve or surface evolving along its normal direction with speed $F > 0$. Let $T(p)$ be the time of arrival of Γ_0 at point p . The function T represents the level set of the evolution of Γ_0 . This function is the solution of the Eikonal equation

$$F \cdot |\nabla T| = 1 \quad (1)$$

with initial condition $T(\Gamma_0) = 0$. The evolution of Γ_0 at time t is the level set t of T .

The Fast Marching Method was introduced by Sethian¹⁹ as an efficient algorithm for solving the Eikonal equation. The algorithm is initialized by manually picking a point inside the saccular volume of the aneurysm. The resulting action map has an abrupt jump in the edges of the object. This allows us to choose an appropriate level set t as a rough pre-segmentation of the object. Due to the features of CTA vessel images, we used a speed based on a vessel enhancement filter.

2.1.1. VESSEL ENHANCEMENT FILTER

A vessel enhancement filter was proposed by Frangi et al.⁷ with the aim of enhancing arteries in MRA and CTA images. This filter computes a pseudo-probability for a voxel of belonging to a tubular structure using geometric properties of the image given by the Hessian matrix. This measure is high inside the tubular structure and nearly zero outside. If $|\lambda_1| \leq |\lambda_2| \leq |\lambda_3|$ are the eigenvalues of the Hessian matrix computed at scale σ , the vesselness function is defined by the formula

$$\nu_\sigma(x, y, z) = \begin{cases} 0, & \text{if } \lambda_2 \geq 0 \text{ or } \lambda_3 \geq 0 \\ (1 - \exp(\frac{-R_A^2}{2\alpha^2})) \exp(\frac{-R_B^2}{2\beta^2})(1 - \exp(\frac{-S^2}{2c^2})), & \text{otherwise} \end{cases} \quad (2)$$

where $R_A = \frac{|\lambda_2|}{|\lambda_1|}$ and $R_B = \frac{|\lambda_1|}{\sqrt{|\lambda_2 \cdot \lambda_3|}}$ are used to distinguish between blob- and line- like structures and S is the Frobenius norm of the Hessian matrix. This parameter uses the additional information that CTA images provide higher values of the filter in the arteries than in the background. The parameters α and β control the sensitivity of the filter for the values of R_A and R_B and were chosen to be 0.5 for all the images. The parameter c controls the sensitivity for the value S and was chosen as 0.25 of the intensity value of the image at the voxel chosen to initialize the Fast Marching algorithm. Changes in the selection of α , β and c were no significant in the final result for all the images.

The speed function used in the Fast Marching algorithm is designed by applying the vessel enhancement filter in a multiscale fashion and calculating the maximum of ν_σ at multiple scales σ . Thus,

$$F(x, y, z) = \max_{\sigma_{\min} \leq \sigma \leq \sigma_{\max}} \nu_\sigma(x, y, z) + \epsilon \quad (3)$$

where ϵ prevents F from being zero.

The speed is maximum at a scale close to the size of the artery or blob to be detected.¹¹ So σ_{\min} and σ_{\max} need to be chosen in the range of the interesting arteries and the width of the saccular region of the aneurysm. The parameter σ_{\min} is chosen equal to 0.03 mm for all images. If bonny structures are located near the aneurysm, σ_{\max} is chosen equal to 0.6 mm. In other case, σ_{\max} is chosen equal to 2.7 mm. The set of scales σ_n is chosen according to an exponential sampling, as suggested by the Scale Space Theory: $\sigma_n = \sigma_{\min} \cdot e^{n \cdot 0.15}$. Thus, no scale is privileged over the others in its contribution to the filter.

Depending on the morphology of the aneurysm and the adjacent bonny structures, the Fast Marching Algorithm provides a pre-segmentation far from the boundaries of the object of interest. In these cases, a freezing algorithm was used to obtain a more accurate pre-segmentation. Freezing algorithm was introduced by Deschamps⁴ as a complement to the Fast Marching algorithm for the segmentation of thin and elongated structures. The main idea of this algorithm is to consider that voxels evolving slowly have reached the boundary of the object, and can be removed from the list of points that are updated according to equation (1). This avoids overpassing the boundaries across the vessels when trying to evolve the front along the artery.

2.2. GEODESIC ACTIVE CONTOURS MODEL

Caselles, Kimmel and Sapiro proposed a model known in the literature as Geodesic Active Contours.² It conciles Parametric Models and the Level Set Theory. This model is based on the idea from geodesic snakes¹⁰ of evolving an initial curve or surface to a local minimum of an energy functional. This functional depends on image terms that attract the front to the edges of the image. Euler-Lagrange equations and the gradient descent method provide the computational framework to evolve the front toward the minimum of the functional. The resulting minimum is a model of the object of interest. The algorithm of level set is used to track the front motion.

The histograms of the images can be modelled as the sum of two Gaussian functions. Due to this fact we use a more sophisticated speed function based on regions and statistical approaches for modelling the motion of the front.

2.2.1. GEODESIC ACTIVE REGIONS

Paragios¹⁶ made a wide study on the inclusion of statistical information in Geodesic Active Contours model. The result was a new model of curve and surface evolution based on region information. The model is based on the idea that a curve or a surface provides a partition of the plane or space in three regions: inside, outside and boundary. Considering the front evolving in the domain of an image, in each time the front Γ provides the following partition:

$$\Omega(t) = \Omega_{in}(t) \cup \Omega_{out}(t) \cup \Gamma(t). \quad (4)$$

Given a partition of the image domain defined by $\Gamma(t)$, we can define its region descriptors. They are functions depending on Ω_{in} , Ω_{out} and the grey level of the image. In this case,

$$k_{in/out}(x, y, z; t) = -\log P_{in/out}(x, y, z; t) \quad (5)$$

where P_{in} and P_{out} are the probabilities for voxel (x, y, z) of belonging to Ω_{in} and Ω_{out} , respectively.

Due to the Gaussian features of the images, these probabilities can be modelled as Gaussian descriptors. So,

$$P_{in/out}(x, y, z; t) = \frac{1}{\sqrt{2\pi}\sigma_{in/out}(t)} \exp\left(-\frac{(I(x, y, z) - \mu_{in/out}(t))^2}{2\sigma_{in/out}^2}\right) \quad (6)$$

where the mean and standard deviation are calculated from the histogram of the image.

Following the ideas of the theory of Geodesic Active Contours, the energy functional associated to the region-based model is defined as

$$E(t) = \zeta \int_{\Omega_{in}(t)} k_{in}(x, y, z; t) dx dy dz + \zeta \int_{\Omega_{out}(t)} k_{out}(x, y, z; t) dx dy dz + \eta \int_{\Gamma(t)} g(x, y, z) d\sigma \quad (7)$$

where $d\sigma$ is the Lebesgue measure on \mathfrak{R} and ζ and η are user defined parameters.

The evolution of the regions in which the domain is divided, can be simplified expressing it in terms of the evolution of the boundary $\Gamma(t)$. So the evolution can be expressed by the partial differential equation

$$\frac{\partial \Gamma(p; t)}{\partial t} = F(p, t) \vec{N} \quad (8)$$

The minimization of the functional $E(t)$ obtained by the Euler-Lagrange equation and gradient descent method is

$$\frac{\partial \Gamma(p; t)}{\partial t} = \zeta(k_{out} - k_{in}) \vec{N} - \eta(g\kappa \vec{N} + \nabla g) \quad (9)$$

So the associated level set equation will be

$$\phi_t + \zeta(k_{out} - k_{in})|\nabla \phi| - \eta(g\kappa|\nabla \phi| + \nabla g \nabla \phi) = 0. \quad (10)$$

2.2.2. NUMERICAL IMPLEMENTATION

The distance transform of the pre-segmentation obtained in the first stage is computed using the Fast Marching Algorithm. This function is used as initial embedding in the Level Set Algorithm. We usually apply 10 iterations of the equation (10) to assure an accurate segmentation. The numerical implementation of the equation (10) depends on the nature of each component:

- ϕ_t : we use forward differences in time to discretize this term.
- $\zeta(k_{out} - k_{in})|\nabla \phi|$: this term acts as a balloon force, so we use an upwind numerical scheme for selecting the correct solution.
- $g\kappa|\nabla \phi|$: this acts as a viscous force, so we use central differences in space to discretize this term.
- $\nabla g \nabla \phi$: this term acts as an advection force, so we use an upwind numerical scheme for selecting the correct solution.

Between each two iterations we force the level set volume be a distance transform. The Sussman-Fatemi algorithm²¹ is applied during 10 iterations and an increment of time of 0.05. This avoids numeric instabilities in the calculation of the curvature.

3. MATERIALS AND METHODS

3.1. ANEURYSMS POPULATION

The study was performed on a data base of 37 patients with ages between 28 and 74 years. The clinical parameters were evaluated in 40 brain aneurysm. The aneurysm were mainly located in the vessels of the Circle of Willis, more specifically in the Anterior Communicating (17), Posterior Communicating (11) and Middle Cerebral (9) Arteries. There were also three aneurysms located in the Carotid (1), Pericallosal (1) and Basilar (1) Arteries.

3.2. IMAGING PROTOCOL

Image acquisition was performed using an Helical Elscint CT Twin scanner (Marconi; Haifa, Israel). Acquisition parameters were 120 kV/300 mA for the amplifier tube, 1.2 mm of collimation with an helical pitch of 1 and slice spacing of 0.6 mm Reconstruction parameters were 512 x 512 matrix with a square FOV of 20.8 cm yielding an in-plane resolution of 0.4 mm A total of 140 ml of non ionic contrast fluid was intravenously administrated (Omnitracst 300 mg; Schering, Berling, Germany) at a rate of 3 ml/s, starting the scanning 20 seconds after injection onset.

3.3. MANUAL MEASUREMENTS

The scanned images were transferred to a SGI Indigo2 workstation (Silicon Graphics, Mountain View, CA) for view and postprocessing. The manual quantification of the aneurysms was performed using 2D Maximum Intensity Images (MIP) and measuring tools provided by the console software Omnipro(Marconi; Haifa, Israel). The clinical parameters needed for the planning of the endovascular intervention were the maximum neck diameter, the width and the depth of the aneurysm. As it is customary in clinical routine, the measurements were carried out along several projection angles and from those, the neuroradiologist chose the view angle producing maximal measurements.

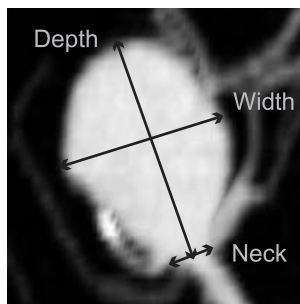


Figure 2. Maximum Intensity Projection image of an aneurysm showing the clinical parameters measured for planning GDC interventions.

3.4. COMPUTERIZED MEASUREMENTS

The output of the devised algorithm is a distance transform of the surface that models the aneurysm and its surrounding vessels. Using the Marching Cubes Algorithm and the VTK visualization library,¹⁸ a 3D visualization of the aneurysm model is obtained automatically. To study the agreement between the manual measurements and the computerized measurements, the rendering viewpoint was the same as for the MIP images and perform the measurements projecting in the camera plane two points from the 3D scene that corresponds to the same magnitude as the 2D scene.

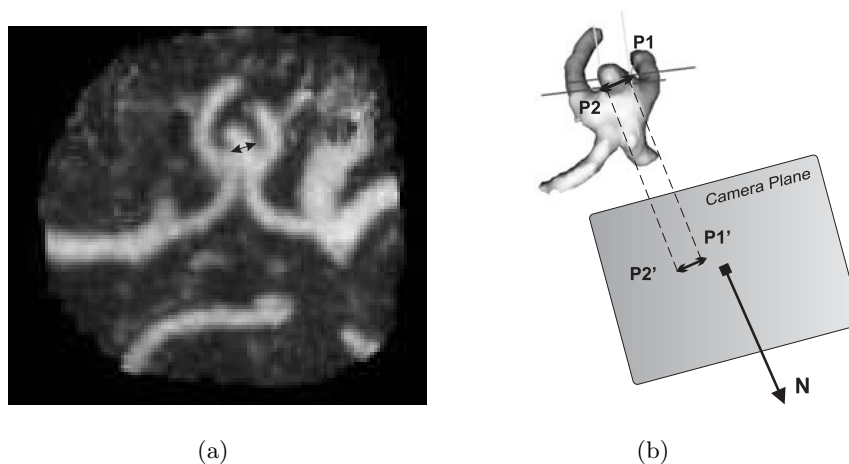


Figure 3. Scheme of the performance of computerized measurements.

4. RESULTS

4.1. EXAMPLES

In Fig. 4 we show some examples of the most representative aneurysms in our data base. The obtained segmentations are visualized using the technique of surface rendering.

4.2. EVALUATION METHOD

The accuracy of the obtained segmentations was studied. Manual measurements were carried out by two experts in two independent sessions. Bland-Altman plots were used as statistical method to obtain the repeatability

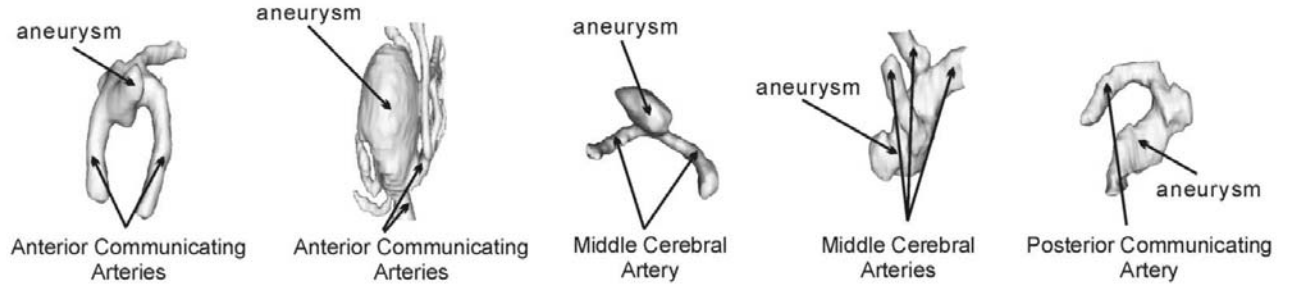


Figure 4. Some representative examples of the segmentations made in the study. (1) Anterior Communicant Artery, (2) Giant Anterior Communicant Artery, (3) Middle Cerebral Artery, (4) Bifurcation of the Middle Cerebral Artery and (5) Posterior Communicant Artery aneurysms.

of the manual method between the two observers and the limits of agreement, $\mu \pm 1.96 \cdot SD$, between manual measurements and the computerized method, where μ is the mean of the differences or bias and SD is the standard deviation of the differences.

4.2.1. MANUAL MEASUREMENTS

Two experts carried out manual measurements of the neck diameter, width and depth of all the aneurysm. All measurements were made twice by each expert with the sufficient delay between sessions to consider them independent. Results of the repeatability of the manual method are shown in Table 1 and Fig. 5. Results of the agreement between the observers are shown in Table 2 and Fig. 6.

4.2.2. COMPUTERIZED MEASUREMENTS

Results of the agreement of the manual method compared with the computerized method is shown in Table 3 and Fig 6.

		Neck [mm]	Width [mm]	Depth [mm]
Bias	ObsI	0.06	1.01	-0.86
	ObsII	-0.44	-0.39	0.12
SD	ObsI	1.16	1.98	2.33
	ObsII	0.93	1.30	1.49

Table 1. Bias and standard deviation of the differences between each observer's session.

	Neck [mm]	Width [mm]	Depth [mm]
Bias	-0.06	0.45	-0.78
SD	0.73	1.11	1.34

Table 2. Bias and standard deviation of the differences between the means of each observer.

	Neck [mm]	Width [mm]	Depth [mm]
Bias	-0.49	0.02	-0.83
SD	0.88	1.38	2.60

Table 3. Bias and standard deviation of the differences between the means of manual observer and computerized method.

5. DISCUSSION

Implicit Deformable Model is a suitable technique for the segmentation of vascular structures because it allows changes in the topology and curvature of the model. However, classic Geodesic Active Contours approach is

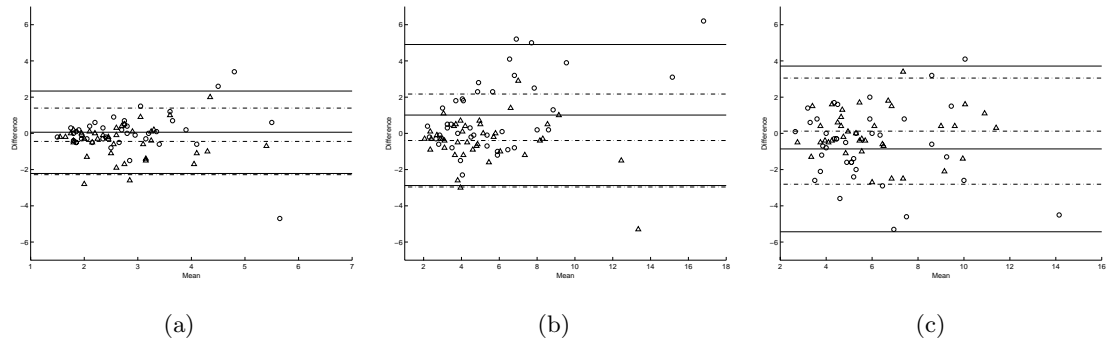


Figure 5. Bland-Altman plot comparing the manual measurements. The symbol \circ stands for ObsI and \triangle for ObsII.

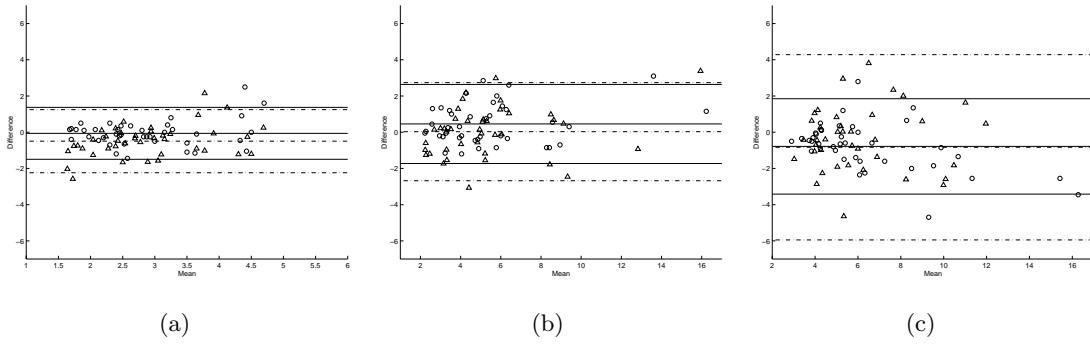


Figure 6. Bland-Altman plot comparing the manual measurements. The symbol \circ stands for manual agreement and \triangle for manual vs computerized agreement.

unsatisfactory for modelling the cerebral vasculature and more sophisticated speed functions need to be added to the classic approach providing better results.

Results obtained with the manual method show that both observers perform similar measurements in independent sessions. The bias is less than 1.01 mm in all the cases. The standard deviation is greater in the measurement of width and depth than neck. This is due to minimal variations in the selection of the angle can provide big variations in the saccular dimensions of the aneurysm extracted from the MIP image. This variations are less significant in the neck due to symmetry.

Inter-observer variability in the manual method presents a negligible bias in neck (-0.06 mm) and less than 1 mm in width and depth. The standard deviation is greater in the measurement of width and depth than neck as happened with intra-observer study. The reasoning of the variability of the angle selection is also applied here. Inter-observer variability of the manual method versus computerized presents slightly higher bias in the measurements of neck and depth than in the manual study and a negligible bias in width (0.02 mm). This bias is in all cases less than 1 mm The standard deviations are slightly higher in neck and width and higher in depth measurements. The reason for this results is that MIP images do not show the real width and depth of the aneurysm and minimal variations on the selected angle provide great variations in the measurements. This effect is higher in the depth magnitude. Nevertheless we consider there were no significant differences in the intra-observer measurements.

In some of the MIP images we observe a misinterpretation of the overlapping vessels with wrong selection of the neck magnitude. In the majority of the cases the real width and depth magnitudes were not measured correctly. We consider that real three dimensional measurement would provide better results in the selection of the appropriate coil size for the surgical intervention.

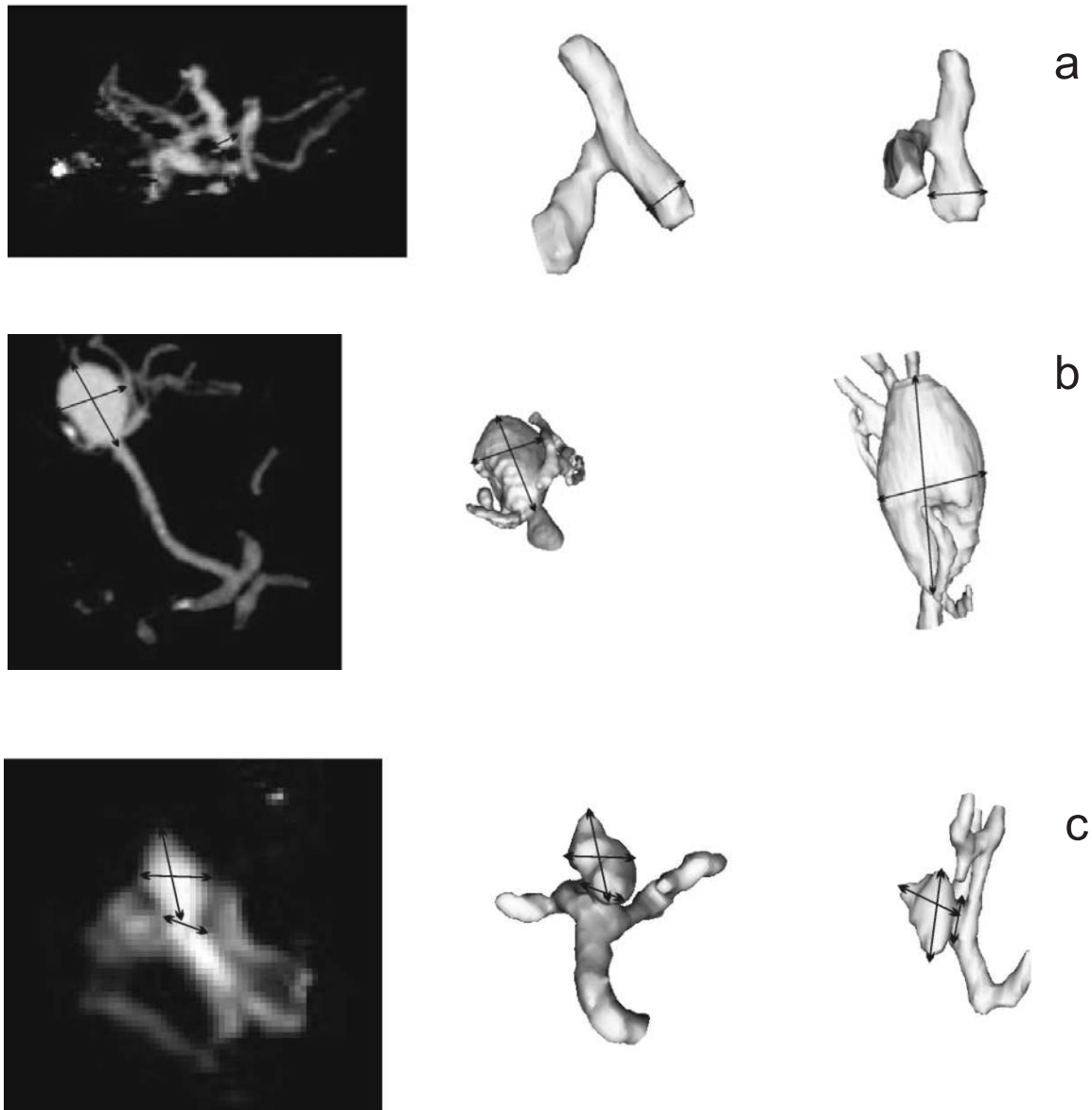


Figure 7. Examples of the limitations of manual measurements. The first column shows the MIPs used for manual measurements. The second column shows a surface rendering computed from the automatic segmentation in the same viewpoint as the MIPs. Finally, the third column shows a surface rendering from an optimal viewpoint interactively selected by an experienced observer. (a,b) Small variations in the viewpoint can lead to large variations in the apparent dimensions of the aneurysm. (c) Overlapping vessels can lead to misinterpretation of the actual dimensions.

6. CONCLUSION

The study reported in this article indicates the feasibility of using Implicit Deformable Models to quantify aneurysm morphology and obtain the clinically relevant parameters. Statistical analysis has shown no statistically significant differences between manual and computerized measurements. In summary, the technique presented in this work will contribute to the computerized pre-surgical planning of coiling procedures by providing more accurate and true 3D quantification of aneurysms morphology.

ACKNOWLEDGMENTS

MHG is supported by the grant AP2001-1678 from the Spanish Ministry of Education, Culture and Sport. AFF is supported by a Ramon y Cajal Research Fellowship from the Spanish Ministry of Science and Technology. This research was partially supported by the grants TIC2000-1635-C04-01, TIC2002-04495-C02 and FIT-070000-2002-935 from the same Ministry.

REFERENCES

1. G.B. Anderson, D.E. Steinke, K.C. Petruk, R. Ashforth, and J.M. Findlay, *Computed Tomographic Angiography versus Digital Subtraction Angiography for the diagnosis and early treatment of ruptured intracranial aneurysms*, *Neurosurgery* **45(6)** (1999 Dec), 1315–20.
2. V. Caselles, R. Kimmel, and G. Sapiro, *Geodesic active contours*, *International Journal of Computer Vision* **22 (1)** (1997), 61–79.
3. G.M. Debrun, V.A. Aletich, P. Kehrl, M. Misra, J.I. Ausman, F. Charbel, and H. Shownkeen, *Aneurysm geometry: an important criterion in selecting patients for Guglielmi detachable coiling*, *Neuro. Med. Chir.* **38** (1998 Apr), 1–20.
4. T. Deschamps, *Extraction de courbes et surfaces par mthodes de chemins minimaux et ensembles de niveaux. applications en imagerie medicale 3d*, Ph.D. Thesis, University of Paris-Dauphine, France (2001 Dec).
5. Z. Dovey, M. Misra, J. Thornton, F.T. Charbel, G.M. Debrun, and J.I. Ausman, *Guglielmi detachable coiling for intracranial aneurysms: the story so far*, *Arch.Neurol.* **58(4)** (2001 Apr), 559–64.
6. A.F. Frangi, W.J. Niessen, P.D. Nederkoorn, J. Bakker, W.P.Th.M. Mali, and M.A. Viergever, *Quantitative analysis of vessel morphology from 3D MR angiograms: in vitro and in vivo results*, *Magnetic Resonance in Medicine* **45(2)** (2001 Feb), 311–22.
7. A.F. Frangi, W.J. Niessen, K.L. Vincken, and M.A. Viergever, *Multiscale vessel enhancement filtering*, *Lecture Notes in Computer Science* **1496** (1998), 130–137.
8. G. Guglielmi, F. Vinuela, I. Spetka, and V. Macellari, *Electrothrombosis of saccular aneurysms via endovascular approach*, *Neruosurg.* **75(1)** (1991 Jul), 1–7.
9. M. Kaminogo, M. Yonekura, and S. Shibata, *Incidence and outcome of multiple intracranial aneurysms in a defined population*, *Stroke* **34(1)** (2003 Jan), 16–21.
10. M. Kass, A. Witkin, and D. Terzopoulos, *Snakes: Active contour models*, *International Journal of Computer Vision* **1(4)** (1988), 321–331.
11. T. Lindeberg, *Feature detection with automatic scale selection*, *International Journal of Computer Vision* **30(2)** (1998), 77–116.
12. F.H. Linn, G.J. Rinkel, A. Algra, and J. van Gijn, *Incidence of subarachnoid hemorrhage: role of region, year, and rate of Computed Tomography: a meta-analysis*, *Stroke* **27(4)** (1996 Apr), 625–9.
13. L.M. Lorigo, O. Faugeras, W.E.L. Grimson, R. Keriven, R. Kikinis, and C.F. Westin, *Co-dimension 2 geodesic active contours for MRA segmentation*, *Lecture Notes in Computer Science* **1613** (1999), 126–.
14. L.M. Lorigo, O.D. Faugeras, W.E.L. Grimson, R. Keriven, R. Kikinis, A. Nabavi, and C.F. Westin., *Curves: Curve evolution for vessel segmentation*, *Medical Image Analysis* **5(3)** (2001), 195–206.
15. A.P. Lozier, E.S. Connolly, S.D. Lavine, and R.A. Solomon, *Guglielmi detachable coil embolization of posterior circulation aneurysms: a systematic review of the literature*, *Stroke* **33(10)** (2002 Oct), 2509–18.
16. N. Paragios, *Geodesic active regions and level set methods: Contributions and applications in artificial vision*, Ph.D. Thesis, University of Nice Sophia-Antipolis, France (2000).

17. T.W. Raaymakers, G.J. Rinkel, M. Limburg, and A. Algra, *Mortality and morbidity of surgery for unruptured intracranial aneurysms: a meta-analysis.*, *Stroke* **29(8)** (1998 Aug), 1531–8.
18. W.J. Schroeder, K.M. Martin, and W.E. Lorensen, *The visualization toolkit (VTK)*, Pearson Education (1997).
19. J.A. Sethian, *A fast marching level set method for monotonically advancing fronts*, *Proc. Nat. Acad. Sci.* **4** (1996), 1591–1595.
20. M. Subasic, S. Loncaric, and E. Sorantin, *3-D deformable model segmentation of abdominal aneurysm*, *Proceedings of SPIE Medical Imaging*, San Diego, USA, (2001).
21. M. Sussman, P. Smereka, and S.J. Osher, *A level set method for computing solutions to incompressible two-phase flow*, *Journal of Computational Physics* **114** (1994), 146–159.
22. F. Tomasello, D. D’Avella, F.M. Salpietro, and M. Longo, *Asymptomatic aneurysms. Literature meta-analysis and indications for treatment.*, *J. Neurosurg. Sci.* **42(1)** (1998 Mar), 47–51.
23. C.M. van Bemmelen, L. Spreeuwiers, M.A. Viergever, and W.J. Niessen, *Level-set based carotid artery segmentation for stenosis grading*, *Lecture Notes in Computer Science* **2489** (2002), 36–43.
24. P.M. White, E.M. Teasdale, J.M. Wardlaw, and V. Easton, *Intracranial aneurysms: CT angiography and mr angiography for detection prospective blinded comparison in a large patient cohort.*, *Radiology* **219(3)** (2001 Jun), 739–49.
25. H.R. Winn, J.A. Jane, J. Taylor, D. Kaiser, and G.W. Britz, *Prevalence of asymptomatic incidental aneurysms: review of 4568 arteriograms*, *J. Neurosurg.* **97(1)** (2002 Jan), 240.